AIP Applied Physics Letters

Effects of ZnO-nanostructure antireflection coatings on sulfurization-free Cu2ZnSnS4 absorber deposited by single-step co-sputtering process

Bao-Tang Jheng, Po-Tsun Liu, Min-Chuan Wang, and Meng-Chyi Wu

Citation: Applied Physics Letters **103**, 052904 (2013); doi: 10.1063/1.4817253
View online: http://dx.doi.org/10.1063/1.4817253
View Table of Contents: http://scitation.aip.org/content/aip/journal/apl/103/5?ver=pdfcov
Published by the AIP Publishing

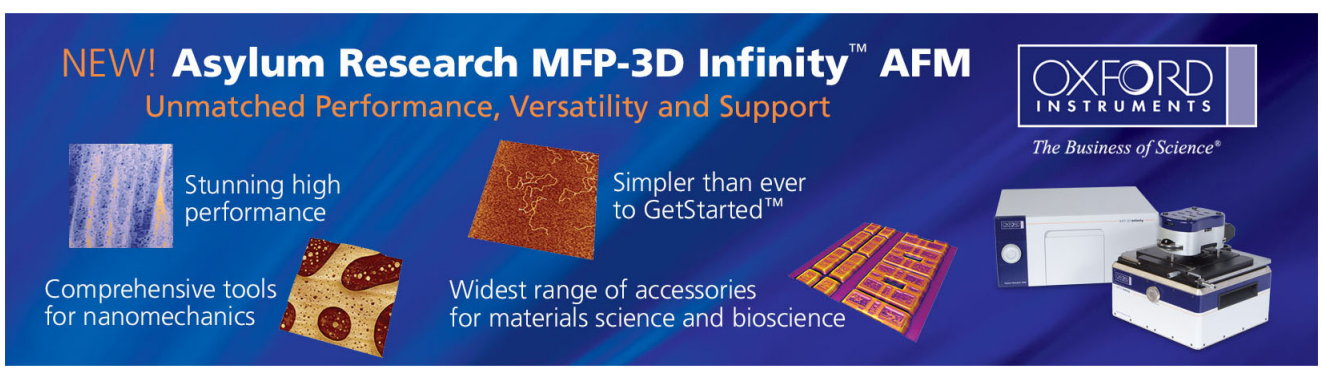

Effects of ZnO-nanostructure antireflection coatings on sulfurization-free Cu_2ZnSnS_4 absorber deposited by single-step co-sputtering process

Bao-Tang Jheng,[1] Po-Tsun Liu,[2,a)] Min-Chuan Wang,[3] and Meng-Chyi Wu[1]
[1]*Department of Electrical Engineering, National Tsing Hua University, Kuang-Fu Road, Hsinchu City, Taiwan*
[2]*Department of Photonics and Display Institute, National Chiao Tung University, Ta-Hsueh Rd., Hsinchu City, Taiwan*
[3]*Physics Division, Institute of Nuclear Energy Research, Taoyuan, Taiwan*

(Received 22 February 2013; accepted 12 July 2013; published online 30 July 2013)

ZnO nanostructures as anti-reflective coatings were synthesized by using hydrothermal technique for a sulfurization-free Cu_2ZnSnS_4 absorber prepared by co-sputtering deposition. By controlling the morphology of solution-grown ZnO nanostructures, the average reflectance of the Cu_2ZnSnS_4 solar cell with branched ZnO nanorods decreased from 7.6% to 1.12%, and the energy conversion efficiency promoted by 10.4% from the initial value of 4.8% to 5.3%. The efficiency improvement was well studied with the effects of the gradually increased refractive index between the air and the top electrode of Cu_2ZnSnS_4 solar device, due to the presence of the ZnO nanostructure. © *2013 AIP Publishing LLC*. [http://dx.doi.org/10.1063/1.4817253]

Solar cells technologies have received a lot of attentions to be applied widely for addressing the energy insufficiency issues that we are facing today. Among the promising candidates of II-VI compounds thin-film solar devices, Cu_2ZnSnS_4 (CZTS) solar cell is potential for photovoltaic (PV) device applications due to many desired features including earth-abundant nontoxic elements, a direct band gap energy of 1.0–1.5 eV, and a large optical absorption coefficient ($>10^4\,cm^{-1}$).[1] It was reported that CZTS solar cells with high energy-conversion efficiency had been fabricated using the hydrazine-based hybrid slurry process.[2] The hydrazine is, however, a highly toxic and rather unstable compound that requires extreme cautions during handling and storage processes. Another leading method to fabricate the CZTS absorber layer is using a two-step sputter-deposited process, in which a post-sulfurization step is followed to be implemented sequentially. In the two-stage sputtering process, metallic precursors with compositional uniformity are required to prepare high-quality CZTS thin films. Several sputtering procedures of stacked-metal or alloy layers, such as Cu/ZnSn/Cu, SnS_2/ZnS/Cu, ZnS/Cu/SnS_2 films, have been investigated to facilitate the compositional uniformity.[3,4] A post-annealing process was followed to be carried out at 500–580 °C under inert gas, sulfur (S) or sulfur hydride (H_2S) atmospheres. The critical issues of the typical two-stage sputtering included the contamination with binary sulfides (various phases of Cu_2S, ZnS, or SnS) and the difficulty to control composition stoichiometry. The simple route herein is a single-step sputtering process that involves no sulfurization, a low production cost, and the absence of a solvent that causes the safety concern. The co-sputtering process using two types of compound targets is thereby developing at the early stage for the single-step sputtering of CZTS thin films. Furthermore, the energy-conversion efficiency of solar cells can be promoted reportedly by the addition of antireflection coatings to the photovoltaic device. Nowadays, various synthesis methods for antireflection coatings have been developed, including vacuum process (e.g., evaporation and sputtering[5]) and non-vacuum process (e.g., electron-beam lithography[6] processes and nanoimprint[7] lithography processes). The main drawbacks like etching, electron-beam lithography, and multiple dielectric film deposition are their high manufacture costs and the fact that those treatments might increase surface recombination losses. As a promising alternative, the single-crystal ZnO nanorods exhibit less deep defects than other thin-film structures and are transparent for photons with energy lower than the bandgap energy of 3.2 eV at room temperature. In addition to the availability of subwavelength structure and its transparency, ZnO dielectric antireflection coating performs an appropriate refractive index ($n = 2$), and ability to form textured coating via anisotropic growth.[8] Therefore, the ZnO nanostructures possess high potential to trap light radiation for the antireflection coatings applications.[9] In this work, a sulfurization-free CZTS solar device technology are developed with a single-step co-sputtering of ternary Cu-Zn-Sn alloy and binary Zn-S alloy targets. The process complexity and manufacture cost could be reduced effectively. In addition, the effects of solution-grown ZnO nanostructures as the antireflection coatings on CZTS absorber are studied mainly for further boosting the energy-conversion efficiency of solar cell device.

Cu_2ZnSnS_4 thin-film solar cell devices were fabricated as followed. A layer of molybdenum (Mo) acting as a back contact was first sputter-deposited on a soda-lime glass substrate with an area of $5 \times 5\ cm^2$. The absorber layer of a 1900-nm-thick CZTS was one-step formed by magnetron co-sputtering of ternary Cu-Zn-Sn alloy target and binary Zn-S alloy targets at a RF power of 80 W, under a pressure of 0.4–1 Pa with Ar gas flow rate of 30–50 sccm. The substrate temperature was held at approximately 500 °C to form

a)Author to whom correspondence should be addressed. Electronic mail: ptliu@mail.nctu.edu.tw. Tel.: 886-3-5712121 ext. 52994. FAX: 886-3-5735601. Present address: Department of Photonics and Display Institute, National Chiao Tung University, CPT Building, Room 412, 1001 Ta-Hsueh Rd. Hsin-Chu 300, Taiwan.

kesterite structure CZTS absorber. After KCN solution pre-treatment, CdS buffer layer was deposited in an aqueous solution containing 100 ml of deionized H_2O and 50 ml of cadmium sulfate in a water bath at 60 °C. It was followed that a 70 nm-thick intrinsic ZnO and 250 nm-thick Al-doped zinc oxide (AZO) layers were DC-sputtered sequentially. Finally, a patterned aluminum grid was deposited on the top of the device to facilitate collecting the photo-generated carriers. Every device with an active area of 0.45 cm^2 was separated from neighboring devices by mechanical scribing. In order to fabricate the antireflection coating on the top surface of the CZTS solar cell, ZnO nanostructures were grown by the hydrothermal method. The reaction chemicals were prepared by mixing of zinc nitrate hexahydrate ($Zn(NO_3)_2 \cdot 6H_2O$) and hexamethylenetetramine ($C_6H_{12}N_4$, HMT) in aqueous solution. After the solution was stirred for 15 min, bare CZTS solar cells were immersed vertically in this solution, and the sealed reaction bottle was heated up to 95 °C. The pH value of the solution was adjusted to the desired value from 6 to 9 by using ammonia.

The CZTS absorber layer co-sputtered by ternary Cu-Zn-S alloy and binary Zn-S alloy targets clearly exhibits the characteristic peaks of kesterite or stannite structure in X-Ray diffraction (XRD) analysis, as shown in Fig. 1. XRD spectra also indicate the CZTS film presents a strong (112) preferred orientation and no extra peaks corresponding to metallic or other compound phases. However, it is difficult to distinguish the structure between kesterite and stannite one due to the fact that the XRD patterns of these two structures differ only slightly in the splitting of high order peaks, such as (220)/(204) and (116)/(312) resulted from the lightly different tetragonal distortion (c/2a).[10] The full width at half maximum (FWHM) of the diffraction peak is rather small, which indicates that the film crystallinity is fairly good. In addition to XRD study, Raman spectroscopy analysis was implemented to characterize the samples fully, as shown in the inset of Fig. 1. It is observed that a strong and sharp quaternary Raman shift at 338 cm^{-1} appeared and was attributed to the characteristic of CZTS film. The Raman spectrum of CZTS absorber includes two small peaks, which are characteristic features of the kesterite structures at 287 cm^{-1} and 368 cm^{-1}, respectively, while the lack of a Raman signal at 476 cm^{-1} reflects the absence of a second-order $Cu_{2-x}S$ phase.[11] In these spectra, no extra phases of other compounds, corresponding to binary copper sulfide SnS_2, ZnS, or Cu_2SnS_3 were observed within the detection limits of Raman analysis.[12] The absence of a second phase can lead to homogeneous optoelectronic properties and a low density of recombination centers, further improving the conversion efficiency of solar cells.

Figure 2 shows scanning electron microscope (SEM) images of ZnO nanostructures synthesized at the pH values of 6, 7, 8, and 9, respectively. Hexagonal ZnO nanorods with radiate patterns of approximately 2000–3000 nm in length and 70–150 nm in diameter were obtained at a pH value of 6, as shown in Fig. 2(a). As the pH value increased to 7, the tips of the ZnO nanorods changed from a flat top [Fig. 2(a)] to a tapered shape [Fig. 2(b)] with the addition of ammonia into the growth solution. The size of the nanorods then decreased to approximately 1000–2000 nm in length and

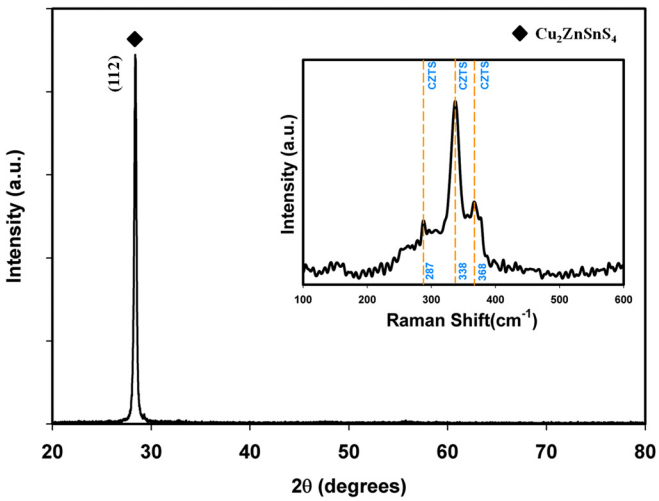

FIG. 1. XRD spectra of the CZTS film formed by co-sputtering targets of Cu-Zn-S and Zn-S alloys. Raman spectroscopy is shown in the inset.

15–50 nm in diameter, while the pH value was at 8, as shown in Fig. 3(c). It is also found that the increase in solution pH value simultaneously decreased both the length and tip diameter of ZnO nanorods in the presence of ammonia, as shown in Fig. 2(b). The shapes of ZnO nanorods developed in a mixture of tip, nanoflakes, and nanoprisms are observed at the pH value of 8 as shown in Fig. 2(c). The flower-like ZnO nanostructures with the length of about 500 nm consisting of multilayered petals are formed as further increasing the pH value to 9. All shapes of flower petals in Fig. 2(d) exhibit the tapering feature with the root size ranging from 500 to 1000 nm and the tip size of 200 nm approximately.

To evaluate the effects of ZnO antireflection coatings on solar cell efficiency, optical and electrical measurements were performed. The absolute hemispherical reflectance measurement system was used to determine full reflectance of ZnO nanostructure layer over the UV–visible range. As shown in Fig. 3, the average reflectance of a bare CZTS solar cell was measured to be 7.6% for the UV-visible wavelength range. Comparatively, the average reflectance of ZnO-nanostructure covered CZTS solar cells with shape patterns of flat top, multi-branched, and branched flower were

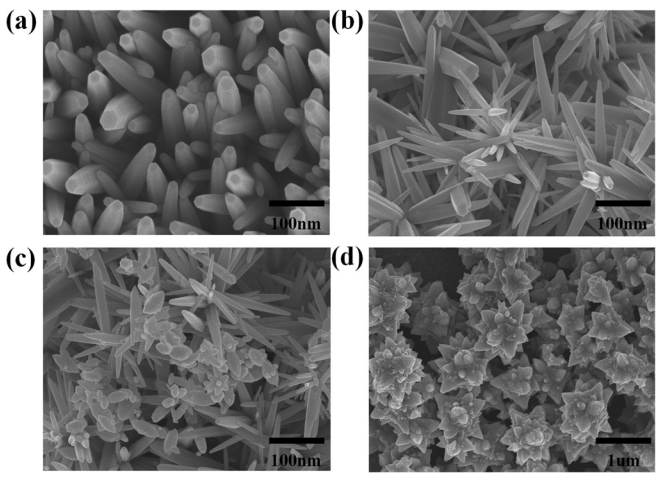

FIG. 2. SEM images of ZnO nanostructures synthesized at different pH values, (a) pH = 6, (b) pH = 7, (c) pH = 8, and (d) pH = 9.

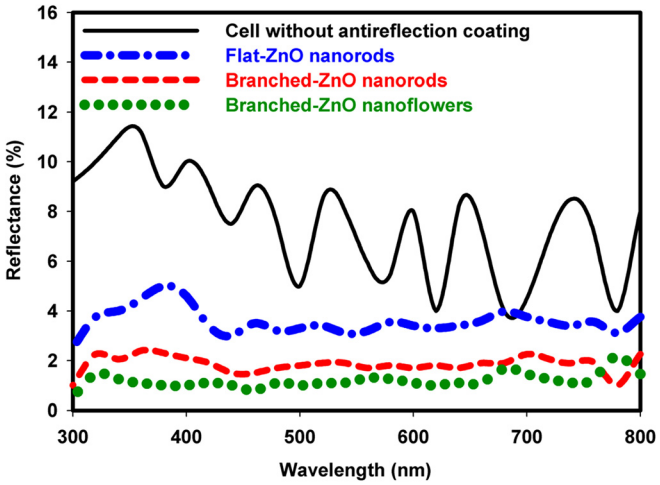

FIG. 3. Optical reflectance spectra of CZTS solar cell devices with different ZnO antireflection coating layers. A bare CZTS solar cell (black), the flat-top ZnO nanorod (blue), the branched ZnO nanorods (red), and the branched ZnO nanoflowers (green).

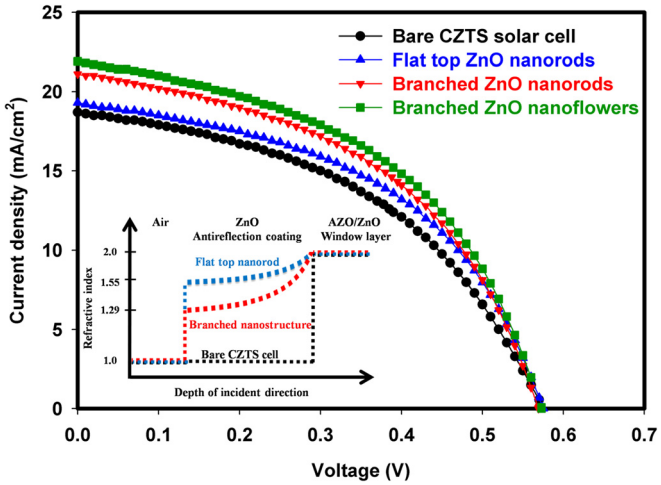

FIG. 4. J-V characteristics of the CZTS solar cells with and without ZnO nanorod antireflection coating layer. This inset shows schematic illustration of refractive index profiles of the surface of CZTS solar cell with different ZnO nanostructures.

measured to be 4.04%, 2.92%, and 1.12%, respectively. As compared with the bare CZTS solar cell, CZTS solar cells with ZnO nanorod array as antireflection coatings exhibited the significantly low reflectance spectra over a wide range of wavelengths, demonstrating its broadband antireflection characteristics. The reflection on CZTS solar cell device was reduced obviously due to the introduction of ZnO-nanorod coating layer. It is thought that the reflectance of ZnO nanorod-coated CZTS cells is independent of wavelengths of the incident photons. Also, the surface morphology of ZnO nanostructures played a key role in the anti-reflectance. Two types of branched ZnO nanorod arrays had lower reflectance spectra compared with the flat one. It indicated that the ZnO nanorods with both of large surface area and decreased top diameter can effectively improved optical antireflection. The elimination of optical interference can be attributed to the fact that the branched nanostructure produces the impedance match between window layer and air through a gradual reduction in the effective refractive index away from the solar cell surface.

Figure 4 shows the characteristics of current density versus voltage (J-V) for the CZTS solar cells with and without ZnO antireflection coatings. The short-circuit current density (J_{sc}) and overall light conversion efficiency (E_{ff}) are increased significantly for the CZTS device with high-density hierarchical ZnO nanowires. The CZTS solar cell with the branched ZnO nanoflowers presented the maximum increase in J_{sc} and E_{ff} by 14% and 12.4%, respectively, in comparison with the bare CZTS solar cell. The increase of J_{sc} was related to the decrease in reflectance. The enhancement of photovoltaic efficiency can be explained by considering a combination of three proposed effects. First, the introduction of multi-branched nanorods as an antireflection coating promoted photon absorption by enhancing light-harvesting without sacrificing efficient photocurrent transport. Second, the coating layer of ZnO nanostructures leads to a continuous refractive index gradient through moth-eye effect between the air and the surface of AZO window layer, as shown in the inset of Fig. 4. Third, the effective refractive index increases with the filling factor (the area ratio of nanorod arrays to the total substrate surface), according to the effective medium theory.[13] The branched ZnO flower-like nanorod arrays are among the lowest effective refractive index at the interface between air and AZO window films, leading to the lowest specular reflectance and interference fringes were not observed at visible wavelength. Thus, the optical reflection at the surface of CZTS solar cell can be suppressed due to the removal of the air-AZO interface by using the subwavelength nanostructure. These results reveal that the ZnO nanostructure effectively absorbed photons owing to its high specific surface area and excellent light-trapping ability.[14–16] Although the efficiency of CZTS solar cell presented in this work is not among the highest value worldwide, it is worthwhile to mention that the hydrothermally grown nanorod arrays are highly promising to be applicable for optimized PV designs since the growth process does not induce physics damages to the device structures.

In summary, the effects of ZnO nanowires as a subwavelength textured antireflection coatings on CZTS thin-film solar cell have been demonstrated in this work. Based on the moth-eye effect, the surface of CZTS solar cell covered with the nanostructured ZnO layer can effectively eliminate optical reflection. The surface morphology of ZnO nanostructures also played a critical role in the reflection reduction. With the coating of branched ZnO nanowires, the average reflectance of the CZTS solar cell decreased by 5.78 times, and the energy conversion efficiency increased by 10.4%. The aqueously grown ZnO nanorods also can be fabricated with a large-area coating process at temperature less than 100 °C. It thereby would have a potential for further application to flexible solar cell technology.

This work was partially supported by Laboratory for Roll to Roll Plasma Coating Technology in Institute of Nuclear Energy Research, Taiwan, under Grant Project No. 1022001INER015.

[1]J. J. Scragg, P. J. Dale, and L. M. Peter, Thin Solid Films **517**, 2481 (2009).
[2]T. K. Todorov, K. B. Reuter, and D. B. Mitzi, Adv. Mater. **22**, E156 (2010).
[3]S. W. Shin, S. M. Pawar, C. Y. Park, J. H. Yun, J. H. Moon, J. H. Kim, and J. Y. Lee, Sol. Energy Mater. Sol. Cells **95**, 3202 (2011).

[4]R. B. V. Chalapathy, G. S. Jung, and B. T. Ahn, Sol. Energy Mater. Sol. Cells **95**, 3216 (2011).
[5]J. K. Kim, A. N. Noemaun, F. W. Mont, D. Meyaard, E. F. Schubert, D. J. Poxson, H. Kim, C. Sone, and Y. Park, Appl. Phys. Lett. **93**, 221111 (2008).
[6]X. Wang, C. J. Summers, and Z. L. Wang, Appl. Phys. Lett. **86**, 013111 (2005).
[7]Z. Yu, H. Gao, W. Wu, H. Ge, and S. Y. Chou, J. Vac. Sci. Technol. B **21**, 2874 (2003).
[8]T. L. Sounart, J. Liu, J. A. Voigt, J. W. P. Hsu, E. D. Spoerke, Z. R. Tian, and Y. Jiang, Adv. Funct. Mater. **16**, 335 (2006).
[9]Y. J. Lee, D. S. Ruby, D. W. Peters, B. B. McKenzie, and J. W. P. Hsu, Nano. Lett. **8**, 1501 (2008).
[10]Q. Guo, H. W. Hillhouse, and R. Agrawal, J. Am. Chem. Soc. **131**, 11672 (2009).
[11]H. Yoo and J. Kim, Sol. Energy Mater. Sol. Cells **95**, 239 (2011).
[12]P. A. Fernandes, P. M. P. Salome, and A. F. da Cunha, Thin Solid Films **517**, 2519 (2009).
[13]P. M. P. Salomé, J. Malaquias, P. A. Fernandes, M. S. Ferreira, A. F. da Cunha, J. P. Leitão, J. C. González, and F. M. Matinaga, Sol. Energy Mater. Sol. Cells **101**, 147 (2012).
[14]D. A. G. Bruggeman, Ann. Phys. **416**, 636 (1935).
[15]Y. C. Chao, C. Y. Chen, C. A. Lin, and J. H. He, Energy Environ. Sci. **4**, 3436 (2011).
[16]H. H. Li, P. Y. Yang, S. M. Chiou, H. W. Liu, and H. C. Cheng, IEEE Electron Device Lett. **32**, 928 (2011).